

Synthesis, Crystallography, and Antibacterial Activity of a New Cocrystal Copper-Cerium Based on 1,10-Phenanthroline

Niloufar Dorosti^{a,*}, Maryam Pass^a and Daniel Fuhrmann^b

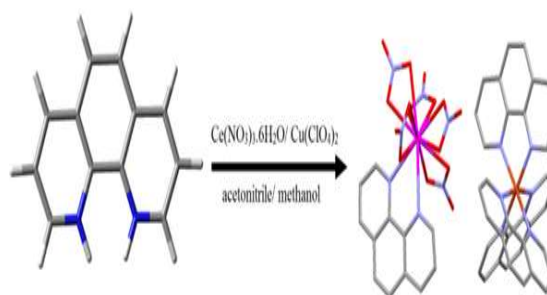
^aFaculty of Chemistry, Lorestan University, Khorram Abad, Iran

^bDepartment of Chemistry and Mineralogy, Institute of Inorganic Chemistry, University of Leipzig, Leipzig, Germany

Received: August 2, 2023; Accepted: September 10, 2023

Cite This: *Inorg. Chem. Res.* **2023**, 7-13. DOI: 10.22036/j10.22036.2023.409813.1150

Abstract: The cocrystal Copper-Cerium based on 1,10-phenanthroline, $[\text{Cu}(\text{Phen})_3][\text{Ce}(\text{Phen})(\text{NO}_3)_5]$ (C), was synthesized by condensation of $\text{Ce}(\text{NO}_3)_3 \cdot 6\text{H}_2\text{O}$, $\text{Cu}(\text{ClO}_4)_2$, and 1,10-phenanthroline in ethanol solution. Newly synthesized cocrystal was characterized by FT-IR, UV-Vis, and elemental analysis. The crystal structure of C was determined by X-ray crystallography. Antibacterial activity of compounds was evaluated against two gram-positive *S. aureus*, *S. saprophyticus* and one gram-negative *P. aeruginosa* bacteria, by the disk-diffusion method. The antibacterial efficacy of the compounds in the concentration range of 10-40 $\mu\text{g}/\text{D}$ is demonstrated by determining the inhibition zone.



Keywords: Cocrystal, X-ray structure, Antibacterial, Hirshfeld analysis

1. INTRODUCTION

Considerable efforts have been devoted to the design and synthesis of cocrystals, in other words crystals composed of two or more distinct molecules in a crystalline lattice, owing to their importance in the pharmaceutical industry.¹⁻³ These compounds show great potential in serving as new antitumor agents.^{4,5} The coordination mode and orientation of the donor groups of organic ligands play an important role in controlling coordination compound structures.⁶ Copper(II) chelates have been found to interact with biological systems and exhibit antineoplastic, antibacterial, antifungal, and anticancer activity.⁷⁻¹⁴ Some Cu(II) N/S, O/N, and N-donor chelators are good anticancer agents due to their strong binding ability with DNA base pairs.¹⁵⁻²⁰ Lanthanide complexes are widely used as optical and magnetic materials, catalysts, and useful in biomedicine.²¹⁻²⁴ Besides, it is well known that lanthanides behave as typical hard acids and prefer donor atoms with the preference $\text{O} > \text{N} > \text{S}$ and $\text{F} > \text{Cl}$.²¹ An overview of the literature shows a wide range of antibacterial activity of Cerium(III) compounds.^{25,26}

The cream or aqueous solution of Ce compounds has been widely used in the antibacterial treatment of burn wounds. Cerium materials cannot penetrate the cell membrane of mammals and no toxicity has been observed with Ce.²⁷ A literature survey reveals that among the different neutral

ligands, 1,10-phenanthroline (Phen) and its derivatives are the subjects of special attention in ternary lanthanide complexes.²⁸⁻³³ 1,10-Phenanthroline is a biologically important ligand, and some of its metal complexes exhibit effective activity against various strains of microorganisms.^{34,35} In this study, the novel cocrystal Copper-Cerium (C) based on 1,10-phenanthroline, was synthesized by condensation of $\text{Ce}(\text{NO}_3)_3 \cdot 6\text{H}_2\text{O}$, $\text{Cu}(\text{ClO}_4)_2$, and 1,10-phenanthroline in ethanol solvent. The resultant Cocrystal was identified *via* IR spectroscopy, elemental analysis, and X-ray Crystallography. In addition, the antimicrobial activity against *S. aureus*, *S. saprophyticus*, and *P. aeruginosa*, was studied by the disk-diffusion method.

2. EXPERIMENTAL

Materials and physical methods

All chemicals and solvents such as 1,10-phenanthroline, $\text{Ce}(\text{NO}_3)_3 \cdot 6\text{H}_2\text{O}$, $\text{Cu}(\text{ClO}_4)_2$, acetonitrile, methanol, and ethanol were of reagent grade and obtained without further purification. Infrared (IR) spectra were recorded on a Shimadzu FT-IR 8400S (Japan) in the range 400-4000 cm^{-1} using KBr pellets. Melting points were measured on an Electrothermal 9100 apparatus. Electronic spectra were recorded by Varian, Cary 100 UV-Vis spectrophotometer in the range of 200-800 nm.

X-Ray structure analysis

Single-crystal X-ray diffraction measurements were carried out on a STOE IPDS 2T image plate diffractometer system equipped with a sealed Mo X-ray tube and a graphite monochromator crystal ($\lambda(\text{MoK}\alpha) = 71.073 \text{ pm}$). Data reduction and numerical absorption correction were carried out with STOE X-AREA software.³⁶ All structures were solved by direct methods using SHELXS-2018 and refined with SHELXL-2018³⁷ using WinGX³⁸ as a graphical frontend. CCDC 2285429 contains the supplementary crystallographic data for this paper. This data can be obtained free of charge via <http://www.ccdc.cam.ac.uk/conts/retrieving.html> (or from the CCDC, 12 Union Road, Cambridge CB2 1EZ, UK; Fax: +44 1223 336033; E-mail: deposit@ccdc.cam.ac.uk).

Antimicrobial Test

The compounds were dissolved in DMSO at the concentration of 1000, 500, and 100 $\mu\text{g/mL}$ and used for antibacterial evaluation. The solution was UV-sterilized and used for disk diffusion. Paper discs (6.5 mm) were impregnated with 40 μL of the sample and the solvent was evaporated under a safety cabinet at room temperature. The bacterial suspension's turbidity was compared and equalized with the Mac-Farland 0.5 standard. Then, the suspension was spread over a Muller Hinton agar plate with sterile swab. The plates were incubated at 35 $^{\circ}\text{C}$ overnight and the inhibition zone (IZ) was measured. The antibacterial effect of **C**, Phen, and metal salts by using the disk diffusion method at 10, 20, and 40 $\mu\text{g/D}$ (microgram per paper discs) concentrations was investigated against two bacteria (*S. aureus*, *S. saprophyticus*) and one gram-negative bacterium (*P. aeruginosa*). DMSO solvent as a negative control and antibiotics Gentamicin and Vancomycin as positive control were considered that microbial shadow created around the disks is the indicative antibacterial effect of compounds.

Synthesis of $[\text{Cu}(\text{Phen})_3][\text{Ce}(\text{Phen})(\text{NO}_3)_5] (\text{C})$

To a solution of 1,10-phenanthroline (Phen) (0.5 mmol, 0.090 g) in 10 mL acetonitrile, $\text{Ce}(\text{NO}_3)_3 \cdot 6\text{H}_2\text{O}$ (0.25 mmol, 0.108 g) and $\text{Cu}(\text{ClO}_4)_2$ (0.25 mmol, 0.092 g) in methanolic solution was added and the resulting mixture was then stirred 72h at room temperature. Green single crystals were obtained by recrystallization from ethanol solution at room temperature. Yield 30%, M.p. 229–230 $^{\circ}\text{C}$; Anal. Calc. for $\text{C}_{48}\text{H}_{32}\text{CeCuN}_{13}\text{O}_{15}$: C, 46.69; H, 2.61; N, 14.74%. Found: C, 46.75; H, 2.65; N, 14.68%. IR (KBr, cm^{-1}): 3070 (s), 1620 (s), 1585 (s), 1442 (w), 1334 (w), 1218 (s), 1141 (s), 1099 (s), 1037 (s), 848 (s), 725 (s), 636 (s). UV-Vis in DMSO: λ_{max} 266 nm.

3. RESULTS AND DISCUSSION

Infrared-Spectra

In the IR spectra of Phen, the absorption bands at 1571 cm^{-1} and 1496 cm^{-1} were assigned to $\nu(\text{C}=\text{N})$ and $\nu(\text{C}=\text{C})$ stretching vibrations, respectively. These bands shifted to lower wavenumber 1512 cm^{-1} and 1438 cm^{-1} in the IR spectra of **C**, which indicate the nitrogen atoms of Phen are coordinated to Ce(III) ion and Cu(II). In addition, the bands at 429 cm^{-1} and 505 cm^{-1} were assigned to $\nu(\text{Cu}-\text{N}_{\text{phen}})$ in the cocrystal.³⁹ Meanwhile, the new bands occurring in the region 420 cm^{-1} $\nu(\text{Ce}-\text{N})$ for

the compound indicate that nitrogen atoms of the Phen group participate in coordination with the Ce(III) ion (Figure 1).⁴⁰

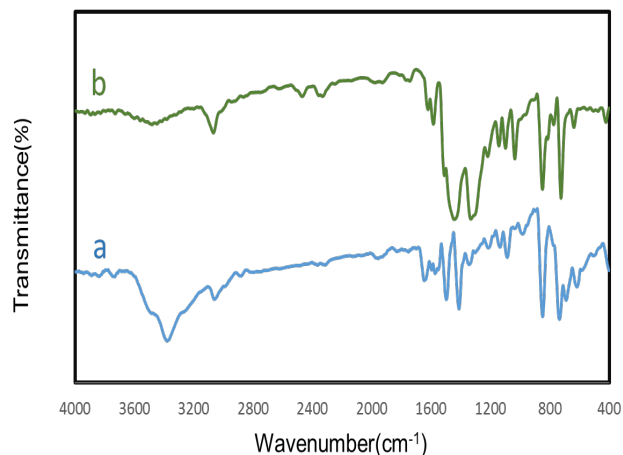


Figure 1. FT-IR spectrum of (a) Phen, and (b) cocrystal C.

Ultraviolet spectra

UV spectra of the Phen and cocrystal **C** are depicted in DMSO solution ($1.0 \times 10^{-5} \text{ mol/L}$) in the wavelength range of 200–400 nm. The **C** and Phen have strong $\pi \rightarrow \pi^*$ transition absorption. The maximum absorption band at 266 nm for the cocrystal **C** is similar to that in the Phen, which indicates that the formation of Ce-N has no conspicuous influence on the UV absorption of the Phen. By changing the solvent to ethanol, the absorption spectrum of Phen and **C** exhibit two relatively strong absorption peaks at 230 and 266 nm, which can be assigned to the $\pi \rightarrow \pi^*$ transition of the Phen ring (Figure 2).

The solvatochromic behavior of cocrystal **C** is the shift of the $\pi \rightarrow \pi^*$ band wavelength due to the presence of solvent with different polarity and interaction between the solute and solvent molecules.

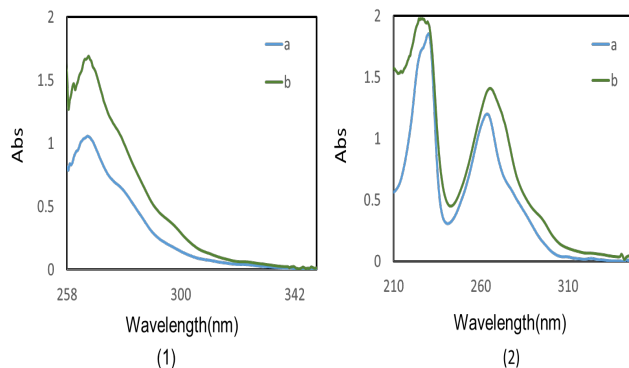


Figure 2. UV-Vis spectra in (a) **C**, and (b) Phen in (1) DMSO and (2) Ethanol.

Description of the molecular structure of cocrystal (C)

Green crystals of (C) were obtained after slow evaporation at room temperature (see Experimental section). Crystallographic data and details of the X-ray analysis are given in Table 1, and the defined dihedral angles and distances of (C) are summarized in Table 2.

Table 1. Crystallographic and Structural Refinement Data for Cocrystal C

Formula	C ₄₈ H ₃₂ CeCuN ₁₃ O ₁₅
Formula weight	1234.52
Temperature (K)	200 K
Wavelength λ (Å)	0.71073
Crystal system	orthorhombic
Space group	P 2 ₁ 2 ₁ 2 ₁
Crystal size (mm ³)	0.438 × 0.346 × 0.267
a (Å)	12.4494(4)
b (Å)	17.9555(5)
c (Å)	22.6236(9)
α (°)	90
β (°)	90
γ (°)	90
Volume (Å ³)	5057.2(3)
Z	4
Density (calcd.) (g cm ⁻³)	1.621
F(000)	2472.0
Absorption coefficient (mm ⁻¹)	1.39
Index ranges h, k, l max	-15 ≤ h ≤ 15, -22 ≤ k ≤ 22, -25 ≤ l ≤ 27
2θ range for data collection/°	3.6 to 52
Unique data (Rint)	9913
Parameters, restraints	703, 0
Final R indexes [I > 2σ(I)]	R ₁ = 0.0518, wR ₂ = 0.1307
Final R indexes [all data]	R ₁ = 0.0653, wR ₂ = 0.1402
Goodness of fit on F ² (S)	1.029
Largest diff peak and hole (e Å ⁻³)	0.96/-1.86

Table 2. Selected bond lengths (Å) and angles (°) in C

Bond lengths (Å)		Bond angles (°)			
Cu1-N3	2.027	Ce1-O9	2.702	N3-Cu1-N4	80.77
Cu1-N4	2.090	Ce1-O10	2.618	N5-Cu1-N6	75.97
Cu1-N5	2.090	Ce1-O11	2.689	N7-Cu1-N8	77.53
Cu1-N6	2.326	Ce1-O13	2.627	N1-Ce1-N2	60.87
Cu1-N7	2.276	Ce1-O15	2.672	O1-Ce1-O2	47.87
Cu1-N8	2.032	O1-N9	1.285	O4-Ce1-O5	47.79
Ce1-N1	2.722	O2-N9	1.246	O7-Ce1-O8	48.56
Ce1-N2	2.764	O4-N10	1.270	O10-Ce1-O11	47.77
Ce1-O1	2.605	O5-N10	1.257	O13-Ce1-O15	48.56
Ce1-O2	2.709	O11-N12	1.278		
Ce1-O4	2.610	O10-N12	1.240		
Ce1-O5	2.737	O15-N13	1.282		
Ce1-O8	2.537	O13-N13	1.266		
O14-H14	2.508	O13-C36	2.707		
O14-C48	3.007	N11-C35	2.879		
O14-C47	3.090				

X-ray analysis showed that C crystallizes in the orthorhombic system P2₁2₁2₁ with four discrete molecules in the unit cell (Figure 3).

The asymmetric unit of (C) contains two symmetry-independent pairs of [Cu(Phen)₃]²⁺ and [Ce(Phen)(NO₃)₅]²⁻ (Figure 4).

Three molecules of Phen are coordinated to the copper(II) ion in a bidentate manner at the nitrogen site of the molecules, and one Phen is attached at the Ce atom. Six-coordinated Cu(II) metal ion has a distorted octahedral geometry (Figure 5). The Cu-N bond lengths lie in the range 2.027(7)–2.326(9) Å in good consonance with the

other reported compounds.⁸ In the asymmetric unit of [Ce(Phen)(NO₃)₅]²⁻, the central Ce ion is 12-coordinated,

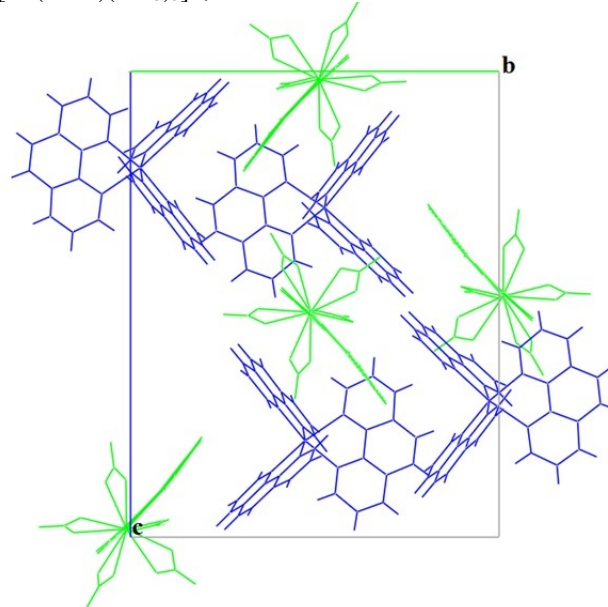


Figure 3. Side view of the crystal packing of C in the bc-plane.

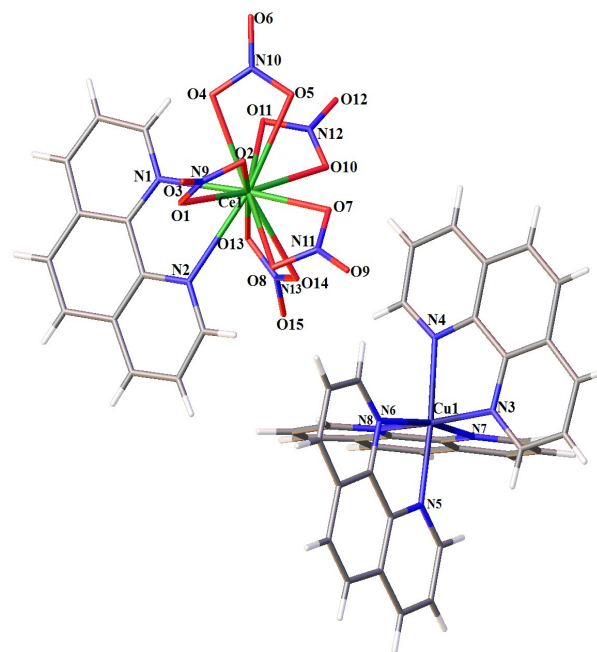


Figure 4. A view of the asymmetric unit and atom-labelling scheme for [Cu(Phen)₃]²⁺[Ce(Phen)(NO₃)₅]²⁻.

made up of two nitrogen atoms of Phen and ten oxygen atoms from five nitrate counter ions; *d* (Ce-O) = 2.537(6) - 2.737(7) Å and *d* (Ce-N) = 2.722(8) - 2.764(8) Å (Table 2 and Figure 4).⁴¹

Non-covalent interactions as weak hydrogen bonds comprising CH_{phen}...O_{nitro} (C(36)–H(36)...O(13): *d*(C36–O13) = 3.623(1) Å, θ(C36–H36...O13) = 162.10(9)°),

(C(24)–H(24)...O(14): $d(\text{C24-O14}) = 3.623(1) \text{ \AA}$, $\theta(\text{C24-H24...O14}) = 162.10(9)^\circ$), (C(19)–H(19)...O(6): $d(\text{C19-O6}) = 3.623(1) \text{ \AA}$, $\theta(\text{C19-H19...O6}) = 162.10(9)^\circ$) (between hydrogens of Phen and O_{nitro}) lead to a two dimensional framework (Figure 5a).

Besides, two neighboring chains are correlated by π - π stacking interactions between aromatic rings of Phen groups (shown in Figure 5b) with centroid–centroid distance of 3.769 \AA and an angle of 10.48° between two planes. There are also weak intramolecular hydrogen bonds between N_{nitro}...CH_{phen} (Figure 5c). Eventually, C adopts a 3D supramolecular structure (Figure 5d).

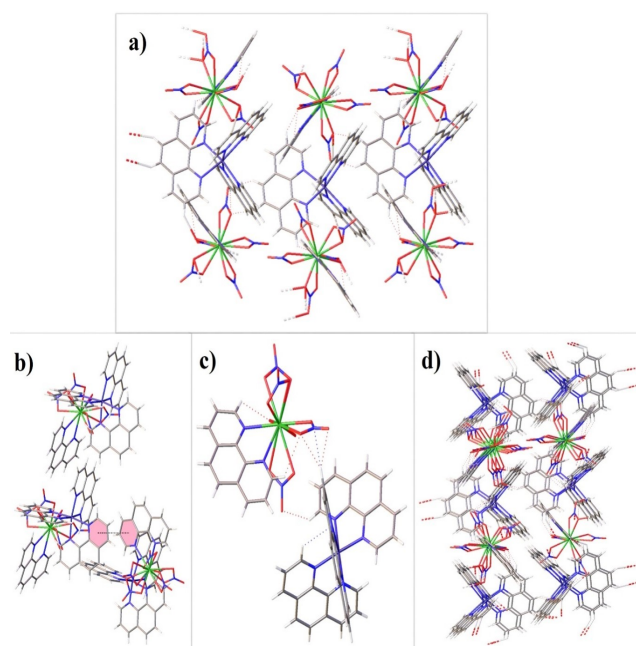


Figure 5. Crystal packing of $[\text{Cu}(\text{Phen})_3]^{2+}[\text{Ce}(\text{Phen})(\text{NO}_3)_5]^{2-}$. (a) A view of short contacts CH...O and CH...N interactions. (b) π - π stacking interactions of the obtained crystal; (c) Side view of intramolecular interaction in C, (d) Representation of interactions in C, resulting in 3D arrangements.

Hirshfeld analysis

Hirshfeld surfaces and molecular fingerprints for cocrystal C was prepared using Crystal-Explorer 3.1, and is presented in Figure 6. Hirshfeld surface analysis is a powerful tool for visualizing and understanding of intermolecular interactions.⁴² The contribution percentage of different interactions to the Hirshfeld surface area is shown in Figure 7. The Hirshfeld surface (HS) mapped with the d_{norm} value of the cocrystal displays the area encoded with different colors, in which the red regions represent the close contacts formed. In contrast, the white-colored regions correspond to weak contacts and the blue-colored areas are considered to be absent of important contacts. Herein, the red areas where the distance between adjacent atoms is shorter than the sum of the van der Waals radii deserve to be highlighted.

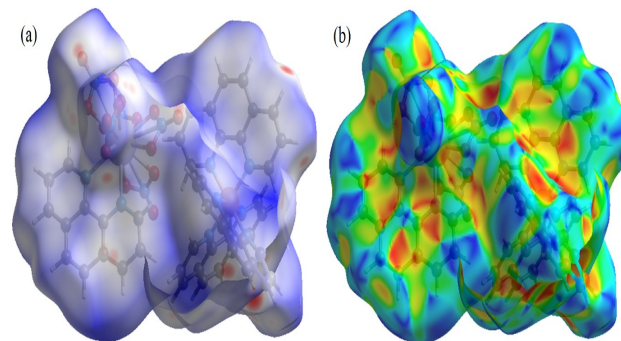


Figure 6. Hirshfeld surfaces mapped with (a) d_{norm} and (b) shape index of C.

Furthermore, 2D fingerprint plots (FPs), derived from the HS, are generated for visualizing percentage contribution of each contact, providing a ‘fingerprint’ of the different intermolecular interactions throughout the structure. Figure 7 shows the overlap of all contact type over the HS of the cocrystal, in which the marked blue color region and length of spikes are indicative of the strength of contacts present in crystal packing. The H...H interactions in Figure 6 are found to be located in the middle of scattered points in the FP and have the (contributions 24.1%) over the total HS as the surface is wrapped in a large number of H atoms. Figure 6 shows that O...H contact, and N-H intermolecular interactions, appears as two sharp long spikes in the FPs. Other contacts, such as C...H, O...C, N...H, and C...C interactions respectively having 20.5%, 4%, 3.8%, and 7.2% are observed. It is clear from the above analysis that the isotropic van der Waals, strong O...H, and weak C...H interactions play major roles in crystal packing.⁴³

percentages of contacts contributed to the total Hirshfeld surface area of C. *de* and *di* refer to distances from the surface to the nearest nucleus exterior and interior to the surface, respectively.

Antibacterial activity

The cocrystal C, Phen, $\text{Ce}(\text{NO}_3)_3 \cdot 6\text{H}_2\text{O}$, and $\text{Cu}(\text{ClO}_4)_2$ were screened for *in vitro* antibacterial activities against *P.aeruginosa*, *S. aureus*, and *S.saprophyticus* by disc diffusion method, and the values of C, Phen, and metal salts are listed in Table 3 and Figure 8. According to the results, all components have activity against *P.aeruginosa* bacterium, resulting in stronger C activity against the titled bacterium compared to the other two bacteria. Besides, the C has significant activities against all the bacteria than Phen and metal salts. This cocrystal has potent activity against *S. aureus* and *S.saprophyticus*, similar to Vancomycin. The obtained data show that Phen is not a biologically active, but its cocrystal with two metal ions Cu(II) and Ce(III) show significantly enhanced activity against bacteria. Previous reports in the literature suggest that the MICs of the La(III) complex are two to

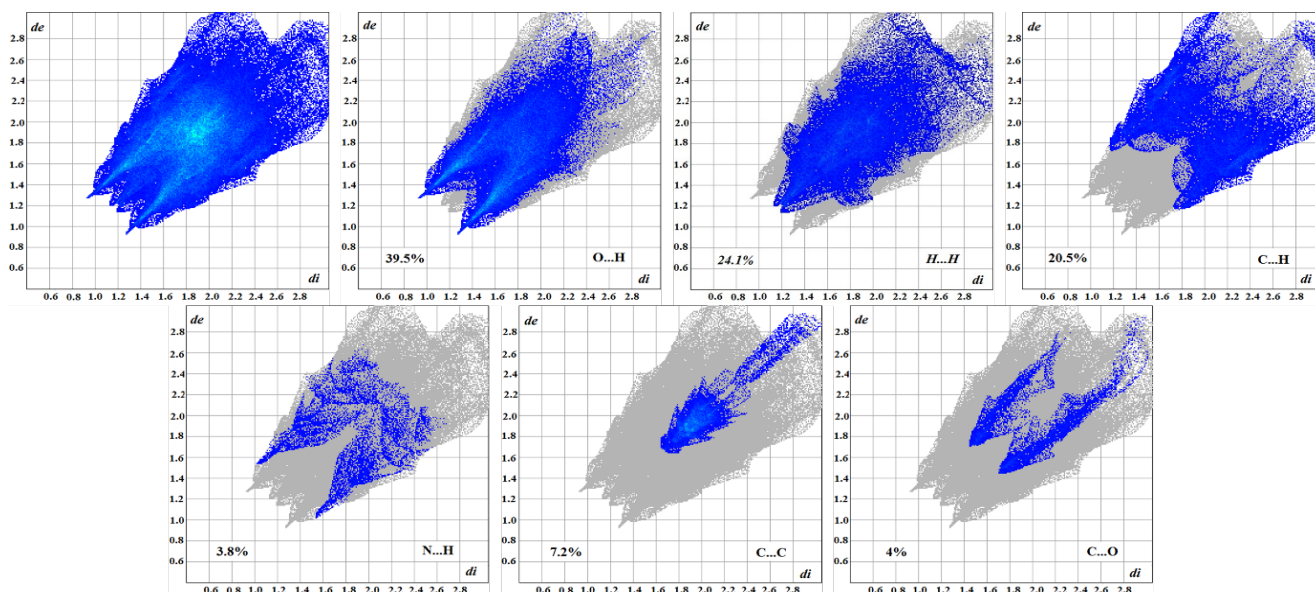


Figure 7. 2D fingerprint plots, full and resolved into O...H, H...H, C...H, C...C, C...O and N...H contacts, showing.

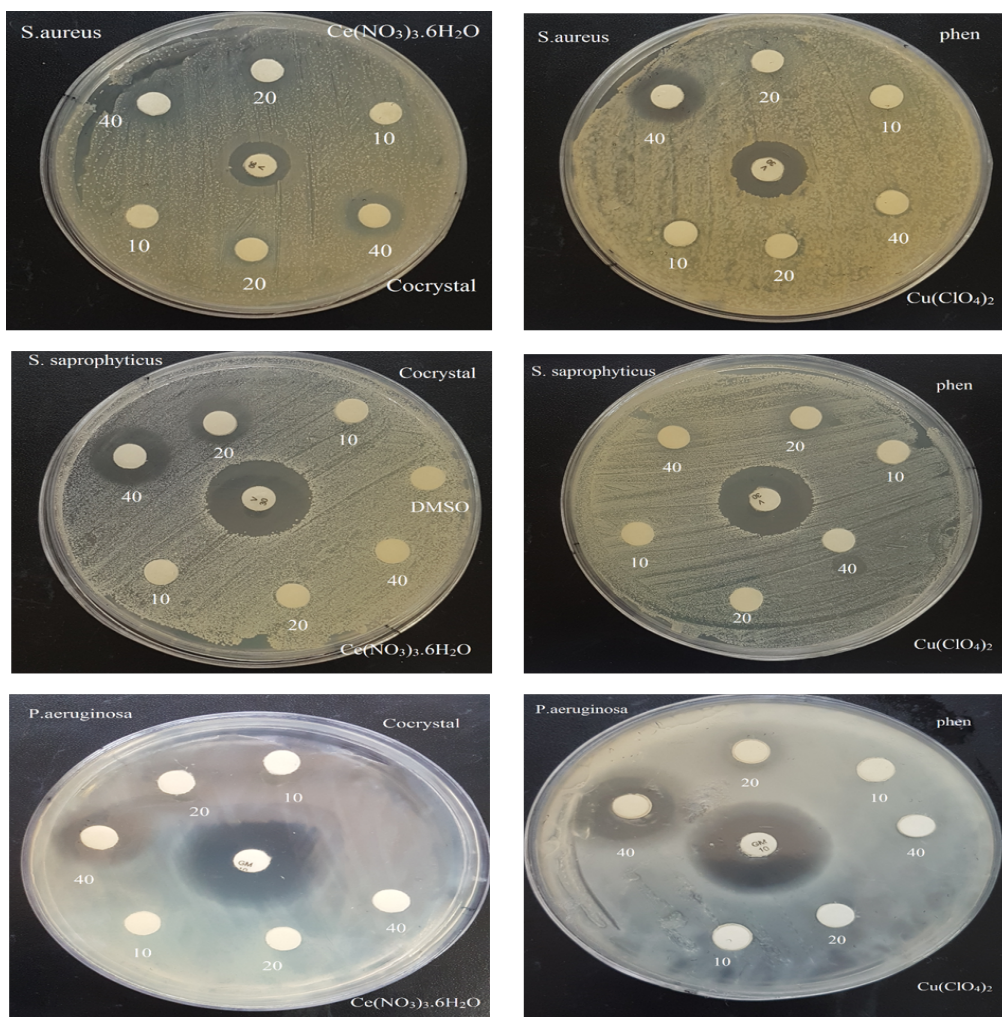


Figure 8. Antibacterial activity of Phen, $\text{Cu}(\text{ClO}_4)_2$, $\text{Ce}(\text{NO}_3)_3 \cdot 6\text{H}_2\text{O}$, and cocrystal C.

Table 3. *In vitro* antibacterial results of Phen, Cu(ClO₄)₂, Ce(NO₃)₃·6H₂O, and cocrystal C

Compound	Inhibition zone in mm			
	concentration µg/D	<i>S. aureus</i>	<i>S. saprophyticus</i>	<i>P. aeruginosa</i>
Phen	10	-	-	-
	20	-	-	15
	40	15	-	20
Cu(ClO ₄) ₂	10	-	-	-
	20	-	-	-
	40	-	-	8
Ce(NO ₃) ₃ ·6H ₂ O	10	-	-	-
	20	-	-	-
	40	-	-	10
C	10	-	-	-
	20	11	15	15
	40	14	18	20
Vancomycin	10	21	15	-
Gentamicin	30	-	-	25

three orders of magnitude smaller than those of the phen and the lanthanum salt (La(NO₃)₃·6H₂O). The results suggest that the La(III) complex has strong antibacterial activity against gram-positive and gram-negative bacteria, implying that the La(III) complex may become a broad-spectrum antibacterial agent.⁴⁴

There are specific reports of Cu(II) complexes where the presence of the copper ion appears to enhance the antimicrobial properties of ligand.⁴⁵

The biological activity of metal compounds may be explained based on the effect of metal ion on the cell metabolism.⁸ The antimicrobial activity of C will increase along with the rise of their concentration in the range of 10–40 µg/D. In contrast, the antimicrobial activity for metal salts in the same concentrations is low. The simultaneous presence of Phen, Cu(II), and Ce(III) in cocrystal C, may be the reason for the potent antimicrobial activity of this compound. Therefore, the result indicates that C has vigorous biological activities which require further research and study to make a useful application in different industries like medicine.

4. CONCLUSIONS

In summary, Cu(II)/Ce(III) cocrystal were successfully synthesized by the reaction of Ce(III) and Cu(II) ions with 1,10-phen in ethanol solvent at room temperature. The crystal structures showed that Phen is coordinated to the metal centers in a bidentate fashion. Furthermore, the *in vitro* antimicrobial activity was evaluated, and the antibacterial effect was conducted by the disk diffusion method, the results of the antibacterial experiments showed that the cocrystal had high activity against the *P. aeruginosa* and *S. aureus* bacteria. The simultaneous presence of Phen, Cu(II), and Ce(III), in the studied cocrystal, maybe the reason for its potent antimicrobial activity. Results demonstrate that the synthesized cocrystal with biological properties might help prevent the progress of various diseases and the development of novel

therapeutic agents.

ACKNOWLEDGMENTS

The authors would like to acknowledge the financial support of Lorestan University for this research under grant number 1401-4-05-3-20-1403.

AUTHOR INFORMATION

Corresponding Author

Niloufar Dorosti: Email: nilufardorosti@gmail.com,
ORCID: 0000-0003-3822-8214

Author(s)

Maryam Pass, Daniel Fuhrmann

REFERENCES

1. K. Moradifard, Z. Derikvand, A. Azadbakht, *Crystallogr. Rep.* **2019**, *64*, 1038-1042.
2. M. Karimi-Jafari, L. Padrela, G. M. Walker, D. M. Croker, *Cryst. Growth Des.* **2018**, *18*, 6370-6387.
3. C. Zhang, Y. Xiong, F. Jiao, M. Wang, H. Li, *Cryst. Growth Des.* **2019**, *19*, 1471-1478.
4. H. Yu, B. Zhang, W. Xing, M. Liu, D. Yang, G. He, F. Wang, L. Zhang, N. Gong, Y. Lu, *Cryst. Growth Des.* **2022**, *22*, 7195-7206.
5. A. Zochedh, M. Priya, A. Shunmuganarayanan, A. B. Sultan, T. Kathiresan, *J. Mol. Struct.* **2023**, *1282*, 135113-135132.
6. Z. Derikvand, A. Azadbakht, B. Notash, *Inorg. Nano-Met.* **2018**, *48*, 196-202.
7. Y. Xu, Y. Shi, F. Lei, L. Dai, *Carbohydr. Polym.* **2020**, *230*, 115671-115695.
8. D. Inci, R. Aydin, T. Sevgi, Y. Zorlu, E. Demirkan, *J. Coord. Chem.* **2017**, *70*, 512-543.
9. A. Abbaszadeh, N. Safari, V. Amani, B. Notash, F. Raei, F. Eftekhari, *IJCCE* **2014**, *33*, 1-13.
10. K. Neethu, S. Sivaselvam, M. Theetharappan, J. Ranjitha, N. Bhuvanesh, N. Ponpandian, M.

- Neelakantan, M. Kaveri, *Inorganica Chim. Acta* **2021**, 524, 120419-120434.
11. K. Ghazal, S. Shoaib, M. Khan, S. Khan, M. K. Rauf, N. Khan, A. Badshah, M. N. Tahir, I. Ali, *J. Mol. Struct.* **2019**, 1177, 124-130.
12. Q. Peña, G. Sciortino, J. -D. Maréchal, S. Bertaina, A. J. Simaan, J. Lorenzo, M. Capdevila, P. Bayón, O. Iranzo and Ò. Palacios, *Inorg. Chem.* **2021**, 60, 2939-2952.
13. N. L. Stevanović, I. Aleksic, J. Kljun, S. Skaro Bogojevic, A. Veselinovic, J. Nikodinovic-Runic, I. Turel, M. I. Djuran, B. Đ. Glišić, *J. Pharm.* **2020**, 14, 24-44.
14. A. Jaafar, A. Fix-Tailler, N. Mansour, M. Allain, W. N. Shebaby, W. H. Faour, S. Tokajian, A. El-Ghayoury, D. Naoufal, J. P. Bouchara, *Appl. Organomet. Chem.* **2020**, 34, 5988-6001.
15. Y. A. Gur'eva, O. A. Zalevskaya, O. G. Shevchenko, P. A. Slepukhin, V. A. Makarov, A. V. Kuchin, *RSC Adv.* **2022**, 12, 8841-8851.
16. S. Sobhani, M. Pordel, S. A. Beyramabadi, *J. Mol. Struct.* **2019**, 1175, 677-685.
17. D. S. Yanick Gaelle, M. Ondoh Agwara, D. M. Yufanyi, J. Nenwa, R. Jagan, *Inorg. Nano-Met.* **2017**, 47, 618-625.
18. P. Yang, D. -D. Zhang, Z. -Z. Wang, H. -Z. Liu, Q. -S. Shi, X. -B. Xie, *Dalton Trans.* **2019**, 48, 17925-17935.
19. D. H. Cai, C. L. Zhang, Q. Y. Liu, L. He, Y. J. Liu, Y. H. Xiong, X. Y. Le, *Eur. J. Med. Chem.* **2021**, 213, 113182-113196.
20. Z. Aguilar-Jiménez, M. González-Ballesteros, S. G. Dávila-Manzanilla, A. Espinoza-Guillén, L. Ruiz-Azuara, *Int. J. Mol. Sci.* **2022**, 23, 12756-12778.
21. L. Zapała, M. Kosińska, E. Woźnicka, Ł. Byczyński, W. Zapała, J. Kalembkiewicz, *Thermochim. Acta* **2018**, 659, 242-252.
22. J. Y. Liu, N. Ren, J. J. Zhang, C. Y. Zhang, *Thermochim. Acta* **2013**, 570, 51-58.
23. N. V. Somov, F. F. Chausov, I. S. Kazantseva, V. L. Vorob'yov, M. A. E. Shumilova, A. N. Maratkanova, *J. Mol. Struct.* **2022**, 1270, 133935-133946.
24. I. Ameen, A. K. Tripathi, R. L. Mishra, A. Siddiqui, U. N. Tripathi, *J. Saudi Chem. Soc.* **2019**, 23, 725-739.
25. Y. -L. Sang, X. -S. Lin, X. -C. Li, Y. -H. Liu, X. -H. Zhang, *Inorg. Nano-Met.* **2017**, 47, 86-90.
26. M. Qi, W. Li, X. Zheng, X. Li, Y. Sun, Y. Wang, C. Li, L. Wang, *Front. Mater. Sci.* **2020**, 7, 213-239.
27. M. Jakupec, P. Unfried, B. Keppler, *Reviews of Physiology, Biochem. Pharmacol.* **2005**, 101-111.
28. P. Nunes, I. Correia, F. Marques, A. P. Matos, M. M. Dos Santos, C. G. Azevedo, J. -L. Capelo, H. M. Santos, S. Gama, T. Pinheiro, *Inorg. Chem.* **2020**, 59, 9116-9134.
29. Y. Wang, C. -W. Jin, S. -M. He, N. Ren, J. -J. Zhang, *J. Mol. Struct.* **2016**, 1125, 383-390.
30. Y. Yang, Z. Zhou, Z. -Z. Wei, Q. -P. Qin, L. Yang, H. Liang, *Dalton Trans.* **2021**, 50, 5828-5834.
31. M. Kosińska-Pezda, L. Zapała, U. Maciołek, Ł. Byczyński, E. Woźnicka, W. Zapała, *JAAP* **2021**, 159, 105293-105251.
32. T. Madanhire, M. C. Pereira, H. Davids, E. C. Hosten, A. R. Abrahams, *Polyhedron.* **2020**, 189, 114713-114728.
33. T. Madanhire, H. Davids, M. C. Pereira, E. C. Hosten, A. R. Abrahams, *Polyhedron.* **2020**, 185, 114583-114594.
34. N. S. Ng, M. J. Wu, J. R. Aldrich-Wright, *J. Inorg. Biochem.* **2018**, 180, 61-68.
35. M. Abaszadeh, R. Hosseinzadeh, M. Tajbakhsh, S. Ghasemi, *J. Mol. Struct.* **2022**, 1261, 132832-132847.
36. STOE & Cie GmbH. X-Area Version 1.70; STOE & Cie GmbH: Darmstadt, Germany, **2014**.
37. G. M. Sheldrick, *Acta Crystallogr. A.* **2008**, 64, 112-122.
38. L. J. Farrugia, *J. Appl. Crystallogr.* **2012**, 45, 849-854.
39. D. S. Yanick Gaelle, M. Ondoh Agwara, D. M. Yufanyi, J. Nenwa, R. Jagan, *Inorg. Nano-Met.* **2017**, 47, 618-625.
40. A. M. Ajlouni, Q. Abu-Salem, Z. A. Taha, A. K. Hijazi, W. Al Momani, *J. Rare Earths* **2016**, 34, 986-993.
41. Y. Y. Zhang, N. Ren, S. L. Xu, J. J. Zhang, D. H. Zhang, *J. Mol. Struct.* **2015**, 1081, 413-425.
42. M. A. Spackman, P. G. Byrom, *Chem. Phys. Lett.* **1997**, 267, 215-220.
43. C. Bejaoui, I. Ameer, N. Derbel, A. Linden, S. Abid, *J. Mol. Struct.* **2018**, 1166, 7-14.
44. S. Gao, M. Huang, Z. Sun, D. Li, C. Xie, L. Feng, S. Liu, K. Zheng, Q. Pang, *J. Mol. Struct.* **2021**, 1225, 129096-129105.
45. Z. Ude, N. Flothkötter, G. Sheehan, M. Brennan, K. Kavanagh, C. J. Marmion, *Int. J. Antimicrob. Agents* **2021**, 58, 106449-106460.